

# Membrane absorption using ionic liquid for pre-combustion CO<sub>2</sub> capture at elevated pressure and temperature



Zhongde Dai, Liyuan Deng\*

Department of Chemical Engineering, Norwegian University of Science and Technology (NTNU), Trondheim 7491, Norway

## ARTICLE INFO

### Article history:

Received 1 April 2016

Received in revised form 24 August 2016

Accepted 1 September 2016

### Keywords:

Pre-combustion

CO<sub>2</sub> capture

Membrane contactor

Ionic liquids

Glass membrane

## ABSTRACT

This study demonstrated the potential of applying ionic liquids as absorbents in membrane contactor for pre-combustion CO<sub>2</sub> capture at elevated temperatures and pressures. Butyl-3-methylimidazolium tricyanomethanide ([Bmim][TCM]) was used as a CO<sub>2</sub> absorbent due to its high thermal stability, moderate viscosity and high CO<sub>2</sub> absorption capacity. The effects of the operating parameters on the CO<sub>2</sub> capture performance in a tubular glass membrane contactor were systematically investigated, including the operating temperature, pressure, and gas flow rate. An overall mass transfer coefficients ( $K_{exp}$ ) value of  $1.0 \times 10^{-6} \text{ m s}^{-1}$  and a CO<sub>2</sub> flux of  $2.50 \times 10^{-4} \text{ mol m}^{-2} \text{ s}^{-1}$  were obtained at an operating temperature of 80 °C and pressure of 20 bar. The  $K_{exp}$  obtained from the experimental characterization were also compared with the  $K_{ov}$  estimated from the resistance in series model.

© 2016 Published by Elsevier Ltd.

## 1. Introduction

CO<sub>2</sub> capture and storage (CCS) is regarded as an effective approach to reduce the effects of anthropogenic emissions on climate change (Abanades et al., 2015; Yang et al., 2008). Efficient membranes/membrane processes are proven effective and promising to deal with CO<sub>2</sub> emissions from power plants in both pre-combustion and post-combustion processes (Dai et al., 2016a; Scholes et al., 2010). Compared to post-combustion CO<sub>2</sub> capture, which aims at the separation of CO<sub>2</sub>/N<sub>2</sub> mixture (~5–15 vol% CO<sub>2</sub>) at a moderate condition, pre-combustion CO<sub>2</sub> capture separates CO<sub>2</sub>/H<sub>2</sub> mixtures with a much higher CO<sub>2</sub> concentration (~45 vol%) at an elevated pressure and temperature. In pre-combustion process, CO<sub>2</sub>/H<sub>2</sub> separation is an important step to purify H<sub>2</sub> from the water-gas shift reaction products and hence avoid CO<sub>2</sub> emission. The selective separation of CO<sub>2</sub> from H<sub>2</sub> at elevated temperatures is the key challenge for this process since this reaction is equilibrium limited and only occurs at appreciable rates at 15–20 bar and temperatures 190–210 °C (Scholes et al., 2010).

Membrane process is considered more energy efficient compared with the conventional physical or chemical adsorption processes commonly used for pre-combustion CO<sub>2</sub> capture in integrated gasification combined cycle (IGCC) power plant. Various attempts have been made to develop membrane process for this

separation. For example, Pd membranes have often been reported as H<sub>2</sub> permeable membranes with very high CO<sub>2</sub>/H<sub>2</sub> selectivity, but Pd membrane is very hard to prepare to an industrial scale and is easily poisoned by the presence of CO and S-compounds. Ceramic membranes are also reported for this application due to their high thermal stability. However, the gas fluxes of ceramic membranes are generally too low for practical applications (Xu et al., 2011), and the fabrication and up-scaling of ceramic membranes/membrane modules are very difficult and expensive. In addition, the purified H<sub>2</sub> in these cases is in the permeate side at low pressures, which requires additional energy for the downstream utilizations of H<sub>2</sub> (usually at high pressures).

Another approach to meet this challenge has been the use of ionic liquids (ILs), an organic salt with negligible vapor pressure and high thermal stability, exhibiting extraordinarily high CO<sub>2</sub> solubility but only negligible H<sub>2</sub> solubility: a CO<sub>2</sub>/H<sub>2</sub> solubility selectivity over 100 was reported (Li et al., 2016; Yokozeki and Shiflett, 2007). The structure of ILs can be specifically designed to have the desired reversible reaction with CO<sub>2</sub> for a highly efficient absorption and easy regeneration through incorporation of selected polar substituents (Ayala et al., 2006; Bara et al., 2008). Gas solubility in ILs shows a strong dependence on temperature and pressure, so are the viscosities of ILs (Anderson et al., 2007; Kurnia et al., 2009). Noble and co-workers have tried to use supported ionic liquids membranes to take advantage of the ILs for CO<sub>2</sub> separation (Bara et al., 2009). However, this ILs membrane only showed a selectivity of 4–20 since H<sub>2</sub> has higher diffusivity than CO<sub>2</sub>. Moreover, according to experiments, this type of ILs supported

\* Corresponding author.

E-mail address: [deng@nt.ntnu.no](mailto:deng@nt.ntnu.no) (L. Deng).

## Nomenclature

$K_{ov,g}$	Overall mass transfer coefficient ( $m s^{-1}$ )
H	Distribution coefficient, dimensionless
$k_l$	Liquid phase mass transfer coefficient ( $m s^{-1}$ )
$k_m$	Membrane phase mass transfer coefficient ( $m s^{-1}$ )
$k_g$	Gas phase mass transfer coefficient ( $m s^{-1}$ )
$k_{mg}$	Mass transfer coefficient of gas filled pores ( $m s^{-1}$ )
$k_{ml}$	Mass transfer coefficient of liquid filled pores ( $m s^{-1}$ )
$d_o$	Outside diameter of the membrane (m)
$d_i$	Inside diameter of the membrane (m)
$d_{ln}$	Log mean diameter of the membrane (m)
$D_g$	Bulk gas diffusivity ( $m^2 s^{-1}$ )
$D_l$	Gas diffusivity in the liquid ( $m^2 s^{-1}$ )
$D_{g,m}$	Effective gas diffusivity in the membrane ( $m^2 s^{-1}$ )
$d_h$	Hydraulic diameter (m)
$v_g$	Gas velocity ( $m s^{-1}$ )
$v_l$	Liquid phase velocity ( $m s^{-1}$ )
L	Length of the membrane (m)
$V_{CO_2}$	Mole volume of $CO_2$ ( $cm^3 mol^{-1}$ )
P	Pressure (bar)
T	Temperature (K)
$N_{CO_2}$	$CO_2$ flux ( $mol m^{-2} s^{-1}$ )
Q	Gas flow rates ( $m^3 s^{-1}$ )
$c_g$	Gas phase $CO_2$ concentrations ( $mol m^{-3}$ )
A	Effective membrane area ( $m^2$ )
$\Delta C_g$	Logarithmic mean concentration (dimensionless)

### Subscripts

g	Gas
l	Liquid
in	Inlet of the contactor
out	Outlet of the contactor

### Greek letters

$\nu$	Kinematic viscosity
$\mu$	Dynamic viscosity of the fluid (Pas or $Ns/m^2$ or $kg m^{-1} s^{-1}$ )
$\rho$	Density of the fluid ( $kg m^{-3}$ )
$\phi$	Membrane wetting ratio (dimensionless)
$\varepsilon_m$	Membrane porosity (dimensionless)
$\delta_m$	Membrane thickness (m)
$\tau_m$	Membrane tortuosity (dimensionless)
$\eta_{IL}$	Kinetic viscosity of the liquid (mPa s)

membranes cannot stand for operations at trans-membrane pressure differences over 2 bar. To overcome the problems in supported ILs membranes while take advantages of the unique properties of ILs, membrane contactor process using ILs as absorbents for  $CO_2$  capture from pre-combustion processes is studied in this work.

Membrane absorption is a hybrid technology combining the advantages of absorption process and membrane technology (Zhang et al., 2013). The main advantages of membrane contactors over conventional packed (random or structured) columns include no flooding and/or foaming, a larger interfacial area, independent operation of the gas and liquid phases, and linear scaling up or scaling down (Ahmad et al., 2010; Li and Chen, 2005). The absorbent is an essential part of a membrane contactor. Many absorbents have been reported in membrane contactors over the past few decades, including alkaline amine solutions (Iliuta et al., 2015; Wang et al., 2004), amino acids salts (Lu et al., 2010), alkaline solutions (Wang et al., 2014), enzyme promoted solutions (Saeed and Deng, 2016; Yong et al., 2015), ammonia solutions (Makhloufi

et al., 2014), and ILs (Dai et al., 2016c; Luis et al., 2009; Wang et al., 2016). Among these absorbents, ILs have unique properties such as negligible volatility, high  $CO_2$  solubility, superior thermal stability, and tailorable structures (Wappel et al., 2010; Zhang et al., 2012), which ensures a higher temperature application and leads to lower solvent loss and lower regeneration energy consumption (Ramdin et al., 2012). Most regeneration processes using an aqueous amine absorbent consume 50–80% of the total energy in the regeneration of the absorbent and the solvent, in which a big portion of the energy is wasted due to solvent evaporation (Kim et al., 2011). Another advantage of ILs is the relatively low corrosion rate and low toxicity. Hasib-ur-Rahman et al. reported the corrosion rate of ILs as being one magnitude or even two magnitudes lower than commonly used amines, such as ethanolamine (MEA) and diethanolamine (DEA) at room temperature (Hasib-ur-Rahman et al., 2012); Papatryfon et al. reported a solvent based on 1-Butyl-3-methylimidazolium tricyanomethanide ([Bmim][TCM]) that exhibited a similar capture performance as DEA 20%, but with much lower corrosiveness and far less toxicity (Papatryfon et al., 2014).

In the past few years, many researchers have tried to apply ILs in membrane absorption processes for gas separation (Albo and Irabien, 2012; Albo et al., 2010, 2011; Gomez-Coma et al., 2014; Jie et al., 2014; Lu et al., 2014; Luis et al., 2009; Ortiz et al., 2010), and most of them relied mainly on quite moderate operating conditions (e.g. ambient pressure/temperature). The influences of different parameters on 1-Ethyl-3-methylimidazolium ethylsulfate ([Emim][EtSO<sub>4</sub>]) and 1-Ethyl-3-methylimidazolium acetate ([Emim][Ac]) have been studied, such as flow rate, temperature, and membrane geometry (Albo and Irabien, 2012; Cadogan et al., 2014; Dindore et al., 2004b; Gomez-Coma et al., 2014). Lu et al. (Lu et al., 2014) studied the performances of  $CO_2$  membrane absorption using two ILs in water solutions, i.e. 1-butyl-3-methyl-imidazolium tetrafluoroborate ([Bmim][BF<sub>4</sub>]) and 1-(3-aminopropyl)-3-methyl-imidazolium tetrafluoroborate ([apmim][BF<sub>4</sub>]). Sirkar et al. studied a pressure swing membrane absorption (PSMAB) process using 1-Butyl-3-Methylimidazolium dicyanamide ([Bmim][DCA]) or its dendrimer-containing solutions as absorbents for  $CO_2$  removal from low-temperature shifted syngas (Chau et al., 2015; Jie et al., 2014). Different from conventional membrane absorption processes where the liquid and gas phase are both circulating, the PSMAB process is more like a pressure swing adsorption process consisting of a six-step cyclic operation, in which the IL absorbent is fixed on the shell side of the membrane module as the stationary phase at a pressure of around 17.2 bar (250 psig) and a temperature of 100 °C.

In this work, a membrane contactor process with closed cycle and continuous flow using ILs as an absorbent was developed for pre-combustion  $CO_2$  capture. In this process, the gas and liquid phases both flow in a steady state at around 20 bar, where  $CO_2$  from the gas phase is selectively absorbed into the ILs in the liquid phase, then the  $CO_2$ -rich liquid stream is sent to a flash tank to relieve part of the pressure, hence part of the  $CO_2$  is released into the flash tank. The partly regenerated IL stream is sent further to a membrane desorber at a reduced pressure and higher temperature to finish the regeneration. Finally, the  $CO_2$  lean IL stream is pumped into the membrane absorber at the higher pressure again (approx. 20 bar) and the whole process forms a closed loop. Helium- $CO_2$  gas mixture (45%  $CO_2$  in helium balance) was used as a surrogate for  $H_2$ - $CO_2$  mixture.  $CO_2/He$  separation data has been commonly used to predict  $CO_2/H_2$  separation performances due to the similar molecular sizes and solubility of  $H_2$  and Helium in various absorbents (Jie et al., 2013, 2014). Furthermore, from the safety point of view, the usage of Helium can avoid the leakage-related problems especially when the process is performed at elevated temperatures and pressures. A report from this work has been published on the com-

parison of using polymeric porous and composite membranes in the membrane contactor. The advantages and disadvantages were analyzed (Dai et al., 2016b).

The present work focuses on the membrane absorption using a porous glass membrane with IL absorbents at elevated temperature and pressure in the designed process. A membrane contactor setup with automatically control and recording system was in-house designed for this work. [Bmim][TCM] and a tubular glass membrane were selected as the CO<sub>2</sub> absorbent and membrane phase, respectively. The effects of the operating parameters on the CO<sub>2</sub> absorption performances were also systematically studied, including gas flow rate (50–200 ml min<sup>-1</sup>), temperature (from room temperature to 80 °C) and pressure (from atmospheric pressure to 20 bar). Moreover, the overall mass transfer coefficients was determined experimentally and were compared with the K<sub>ov</sub> estimated from the resistance in series model with and without wetting. The contributions of the mass transfer resistances from gas, membrane and liquid phases were also analyzed.

## 2. Mass transfer in a membrane contactor

In membrane absorption the overall gas mass transfer encounters three resistances, i.e. gas film resistance, membrane resistance, and liquid film resistance. For a membrane contactor with gas on the shell side and liquid absorbent on the lumen side, the overall transfer coefficient on the basis of the overall gas phase molar concentration difference (K<sub>ov</sub>) can be expressed through a resistance in series model (Khaisri et al., 2009):

$$\frac{1}{K_{ov}} = \frac{1}{Hk_l} + \frac{d_o}{k_m d_{ln}} + \frac{d_o}{k_g d_i} \quad (1)$$

Where K<sub>ov</sub> is the overall mass transfer coefficient (m s<sup>-1</sup>), k<sub>l</sub>, k<sub>m</sub>, and k<sub>g</sub> represent the liquid phase, membrane phase, and gas phase mass transfer coefficient (m s<sup>-1</sup>), respectively, while d<sub>o</sub>, d<sub>i</sub>, and d<sub>ln</sub> are the outside, inside, and log mean diameters of the membrane, respectively. H is the distribution coefficient (dimensionless) and can be calculated as from Eq. S(1) in the Supporting information.

### 2.1. Mass transfer in the gas phase

For gas flowing on the shell side parallel to the membrane, the mass transfer coefficient in the gas phase can be estimated as shown in Eq. (2) (Li and Chen, 2005):

$$k_g = 1.25 \left( \frac{\nu}{D_{g,b}} \right)^{1/3} \left( \frac{d_h^2 \nu_g}{L \nu} \right)^{0.93} \frac{D_{g,b}}{d_h} \quad (2)$$

Where  $\nu_g$  is the kinematic viscosity (m<sup>2</sup> s<sup>-1</sup>) and can be expressed as  $\nu_g = \frac{\mu_g}{\rho_g}$ ,  $\mu_g$  is the dynamic viscosity of the gas (Pa s or N s m<sup>-2</sup> or kg m<sup>-1</sup> s<sup>-1</sup>), and  $\rho_g$  is the density of the gas (kg m<sup>-3</sup>). d<sub>h</sub> is the hydraulic diameter (m),  $\nu_g$  represents the gas velocity (m s<sup>-1</sup>), L denotes the length of the membrane (m), and D<sub>g,b</sub> is the bulk gas diffusivity (m<sup>2</sup> s<sup>-1</sup>), which can be calculated from Eq. S(3).

### 2.2. Mass transfer in the membrane phase

Mass transfer coefficient in the membrane phase can be expressed as Eq. (3) (Kreulen et al., 1993):

$$\frac{1}{k_m} = \frac{1}{k_{mg}} (1 - \phi) + \frac{H}{k_{ml}} \phi \quad (3)$$

Where k<sub>mg</sub> and k<sub>ml</sub> are the mass transfer coefficient of the gas-filled pores (m s<sup>-1</sup>) and liquid-filled pores (m s<sup>-1</sup>), respectively.  $\phi$  is the membrane wetting ratio, referring to the percentage of the

**Table 1**  
Specifications of the membrane contactor.

Parameter	Value
Membrane module length (mm)	300
Effective membrane length (mm)	260
Membrane i.d. (mm)	10
Membrane o.d. (mm)	10.4
Number of membranes	1
Pore size (nm)	100
Porosity	0.57



Fig. 1. SPG glass tubular membrane and membrane module.

total length of all the pores filled with the liquid, and k<sub>ml</sub> can be calculated from Eq. (4):

$$k_{ml} = \frac{D_l \varepsilon}{\delta_m \tau} \quad (4)$$

Where D<sub>l</sub> is the gas diffusivity in the liquid (m<sup>2</sup> s<sup>-1</sup>) and  $\varepsilon_m$  is the membrane porosity,  $\delta_m$  is the membrane thickness (m),  $\tau_m$  is the membrane tortuosity (dimensionless), and k<sub>mg</sub> can be calculated from Eq. (5) (Boributh et al., 2011):

$$k_{mg} = \frac{D_{g,m} \varepsilon}{\delta_m \tau} \quad (5)$$

Where D<sub>g,m</sub> is the effective gas diffusivity in the membrane (m<sup>2</sup> s<sup>-1</sup>) and can be calculated from Eq. S(4).

### 2.3. Mass transfer in the liquid phase

Mass transfer coefficient k<sub>l</sub> in the liquid phase can be expressed using the Leveque correlation (Yang and Cussler, 1986) as shown in Eq. (6):

$$k_l = 1.62 \left( \frac{d_i^2 \nu_l}{D_l L} \right)^{1/3} \frac{D_l}{d_i} \quad (6)$$

Where  $\nu_l$  is the liquid phase velocity (m s<sup>-1</sup>), D<sub>l</sub> is the gas diffusivity in liquid (m<sup>2</sup> s<sup>-1</sup>) and can be calculated from Eq. S(6), d<sub>i</sub> is the inner diameter of the membrane (m), and D<sub>l</sub> is the CO<sub>2</sub> diffusivity in [Bmim][TCM], which can be obtained from Eq. S(6).

## 3. Experimental

### 3.1. Materials

The [Bmim][TCM] was purchased from Iolitec (Germany) and used without further purification. The nitrogen (99.99%) and gas mixture (45% CO<sub>2</sub> in helium balance) cylinders were purchased from AGA (Norway). The microfiltration glass membranes (tubular geometry) and membrane module were purchased from SPG Technology Co. Ltd, Japan. The surface of the skin layer was specially treated to be hydrophobic by the supplier. The specifications of the membrane and membrane contactor are shown in Table 1.

Fig. 1 shows the SPG tubular membrane and membrane module. Instead of the commonly used glue-sealing method, this module

employs four O-rings to seal the membrane with metallic membrane housing.

### 3.2. Materials characterization

The thermal stability of the materials used in the present research was investigated with a thermo-gravimetric analyzer (Q500, TA instrument). Samples with the amount of around 10 mg were tested with a N<sub>2</sub> sweep flow of 60 ml min<sup>-1</sup> and a heating rate of 10 °C min<sup>-1</sup>. In addition, in order to investigate the wettability of the membrane in the presence of the [Bmim][TCM], the contact angle of the [Bmim][TCM] on the membrane was measured by using a contact angle goniometer (Attension Theta, Biolin scientific). A liquid drop with a volume of 3–5 ml was used, and the contact angle was calculated by averaging the left and right contact angles. The possible morphological change of the membrane surface on the liquid contact was investigated through a scanning electron microscope (SEM, TM3030 Tabletop Microscope, Hitachi High Technologies America, Inc). The samples were sputter coated with gold for 1.5 min prior to the SEM to ensure a good electronic conductivity. In the SEM study, an electron beam intensity of 15 kV was employed and a back-scattered electron (BSE) signal was used.

### 3.3. Experimental setup

An in-house-made membrane contactor test rig suitable for elevated temperatures (up to 200 °C) and pressures (up to 20 bar) was used to investigate the performances of the membrane absorption under various conditions (as illustrated in Fig. 2).

The feed gas mixture (CO<sub>2</sub>/He 45/55 vol.%) and the ILs were fed through the shell side and lumen side of the tubular membrane counter-currently. A 2L piston accumulator (Parker, Norway) instead of a pump was employed to inject the liquid into the system. This device enabled the system to maintain a high pressure (up to 20 bar) with a small flow rate (e.g. 10–20 ml min<sup>-1</sup>) and to avoid fluctuation as well as to precisely control the operating parameters in a broad range. The gas and liquid flow rates were controlled by two mass flow controllers (Bronkhorst, Netherland). The gas and liquid side feed pressures were controlled by two back-pressure controllers (Swagelok, Norway) installed downstream of the membrane module, and the pressure could be adjusted between 1–20 bar. The gas and liquid phase pressures were measured by four digital manometers (Keller, DA-35XHTC, precision: 0.5% full scale, Switzerland). To avoid any liquid getting into the gas analyzer in case of breakthrough of the liquid into the gas phase, the gas phase outlet was connected to a liquid trap. The membrane module was placed in a ventilated oven with a temperature control from room temperature to 80 °C. Both the liquid and gas feed were pre-heated before being sent to the membrane absorber. The temperatures were detected by two temperature sensors (Max Sievert, Pt100 3-wire Clas A element, precision: ±0.2 °C) to make sure the feed reached the desired temperature before being sent to the absorber. The compositions of the gas mixture in the feed and in the retentate were analyzed using an on-line gas analyzer (GSM810, SICK AG, Germany).

The CO<sub>2</sub> absorption flux and overall mass transfer coefficient can be calculated by Eqs. (7) and (8), respectively (Wang et al., 2005).

$$N_{\text{CO}_2} = \frac{Q_{g,i}c_{g,i} - Q_{g,o}c_{g,o}}{A} \quad (7)$$

$$N_{\text{CO}_2} = K_{\text{exp}}\Delta C_g \quad (8)$$

Where  $Q_{g,i}$  and  $Q_{g,o}$  are the inlet and outlet gas flow rates in m<sup>3</sup> s<sup>-1</sup>, respectively,  $c_{g,i}$  and  $c_{g,o}$  represent the gas phase CO<sub>2</sub> concentrations in mol m<sup>3</sup> at the inlet and outlet, respectively, which are calculated using the sour SRK model from Aspen Hysys (Yokozeki

et al., 2008), and  $A$  denotes the active membrane area in m<sup>2</sup>.  $\Delta C_g$  is the logarithmic mean driving force based on the gas-phase concentration, and can be described as in Eq. (9):

$$\Delta C_g = \frac{c_{g,i} - c_{g,o}}{\ln\left(\frac{c_{g,i}}{c_{g,o}}\right)} \quad (9)$$

## 4. Results and discussion

### 4.1. Ionic liquid and membrane screening and characterization

#### 4.1.1. Ionic liquid screening and characterization

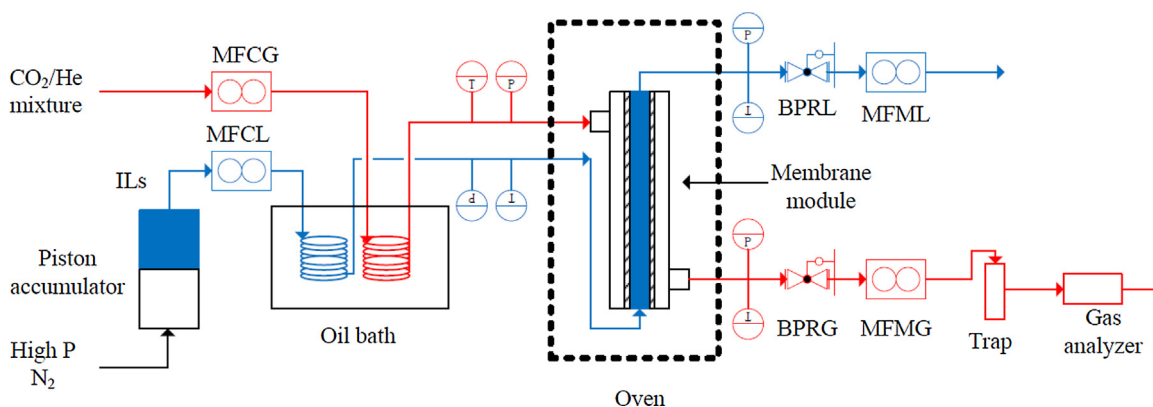
The selection of the absorption liquid is a key in achieving an efficient selective separation. There are many different properties that need to be considered for a qualified absorbent candidate, including thermal and chemical stability, viscosity, CO<sub>2</sub> solubility and selectivity over other gases. In the absorbent selection, all these aspects are needed to be considered. However, no perfect candidate can fulfill all these requirements, so the target in this study is to find an optimized combination of these properties. Imidazolium-based ILs, especially [Bmim] (1-butyl-3-methylimidazolium)-based ILs, are the most commonly studied ILs for CO<sub>2</sub> absorption. Several [Bmim]-based ILs were selected and their properties are listed in Table 2 for comparison. Henry's law constant is used to express gas solubility in physical absorption ionic liquids (Anthony et al., 2002b; Lei et al., 2014). A smaller Henry's law constant value denotes higher gas solubility.

Table 2 lists the CO<sub>2</sub> solubility, thermal stability ( $T_{\text{on-set}}$ ), and viscosity of several [Bmim]-based ILs. As shown in Table 2, [Bmim][TCM] shows much lower viscosity at room temperature compared to other commonly used ILs such as [Bmim][BF<sub>4</sub>], [Bmim][PF<sub>6</sub>], and [Bmim][Tf<sub>2</sub>N]. Only [Bmim][DCA] shows a comparable viscosity to [Bmim][TCM] but with a lower CO<sub>2</sub> sorption capacity in view of the larger Henry's law constant. In terms of CO<sub>2</sub> solubility, [Bmim][TCM] shows a relatively lower Henry's law constant (4.84 MPa) compared to other ILs, with the only exception of the [Bmim][Tf<sub>2</sub>N] (3.30 MPa), which, however, has a 3 times higher viscosity. Overall, compared to other physical ionic liquids considered for the application, [Bmim][TCM] holds the lowest viscosity, reasonably good thermal stability and high CO<sub>2</sub> solubility, is thus selected as the CO<sub>2</sub> absorbent in this study.

The long-term thermal stability of [Bmim][TCM] at 80 °C, 100 °C, and 150 °C was tested in the TGA for 300 min, detailed results were shown in Fig. S1(B). In the three thermal stability tests, the weight loss percentage of all the samples was lower than 0.2% after 6 h, and no color change in the solvents was observed, meaning that [Bmim][TCM] has long-term thermal stability for an operating temperature up to 150 °C.

#### 4.1.2. Membrane screening and characterization

Selecting a good membrane is logically important for an efficient membrane contactor. Through proper surface modification, inorganic membranes (e.g. ceramic membrane, SPG (Shirasu-porous-glass)) glass membrane can gain fairly good hydrophobicity and high contact angles (Koonaphattleert and Li, 2007; Vladislavjevic et al., 2005). In addition, inorganic membranes normally have better thermal and chemical stability compared to polymeric membranes, which is of critical importance for high-temperature applications. Glass membranes feature a uniform pore size and high porosity, and their glass surface can easily be treated to be hydrophobic (Vladislavjevic et al., 2005). These are important characteristics for membrane contactor applications to prevent membrane pore-wetting. In the present study, a hydrophobic SPG glass membrane purchased from SPG Technology Co. Ltd, Japan was used. This membrane has a much higher porosity as well as a much sharper pore size distribution compared to many ceramic mem-



**Fig. 2.** Schematic representation of the experimental membrane contactor setup used for the CO<sub>2</sub>/He separation. MFCG and MFCL represent the mass flow controller for gas and liquid, BPRG and BPRL denote the backpressure regulator for gas and liquid, and MFMG and MFML are the mass flow meter for gas and liquid, respectively. P and T represent the pressure and temperature sensors.

**Table 2**

Comparison of the different properties of [Bmim]-based, commercially available ILs at room temperature.

ILs	Viscosity (mPa s)	T <sub>on-set</sub> (°C)	H <sub>CO2</sub> (MPa)	H <sub>H2</sub> (MPa)
[Bmim][BF <sub>4</sub> ]	132 (Tomida et al., 2006)	380 (Erdmenger et al., 2008)	5.58 (Camper et al., 2006)	197.4 (Jacquemin et al., 2006)
[Bmim][PF <sub>6</sub> ]	382 (Tomida et al., 2006)	349 (Huddleston et al., 2001)	5.34 (Anthony et al., 2002a)	435.0 (Sharma et al., 2009)
[Bmim][Tf <sub>2</sub> N]	100 (Ohno and Yoshizawa, 2002)	427 (Tokuda et al., 2005)	3.30 (Anthony et al., 2005)	133.4 (Jacquemin et al., 2007)
[Bmim][DCA]	28.8 (McHale et al., 2008)	300 (Fredlake et al., 2004)	5.59 (Carvalho et al., 2009)	–
[Bmim][TCM]	27.8 (Zubeir et al., 2015)	334.55 (Zubeir et al., 2015)	4.84 (Zubeir et al., 2015)	–

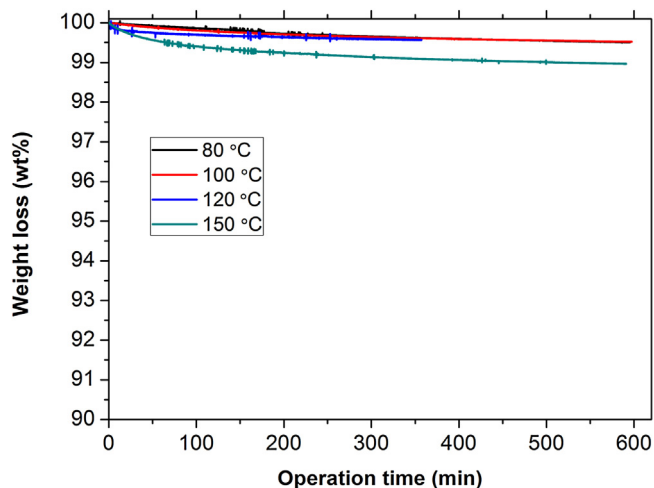


**Fig. 3.** Thermal stability test of the SPG glass membrane at different temperatures.

branes (Table 1). The long-term high-temperature stability of the membrane was tested for 10 h at 150 °C through a TGA experiment as shown in Fig. 3.

The weight loss of the glass membrane at temperatures lower than 120 °C over the investigated period was less than 0.4% over 10 h. After an initial decrease likely related to the residual moisture in the porous structure, a negligible weight loss was observed. Even after increasing the temperature to 150 °C, the weight loss over 10 h remained less than 1%, demonstrating a good thermal stability of the glass membrane for temperatures higher than the maximum operating temperature considered in the present study (80 °C).

The surface morphology was characterized through SEM analysis in order to study the effect of the contact between the [Bmim][TCM] and the glass membrane under elevated temperatures. The surface and the cross-section of the glass membrane before and after being tested for several runs were studied by SEM and the results can be found in Fig. S2.

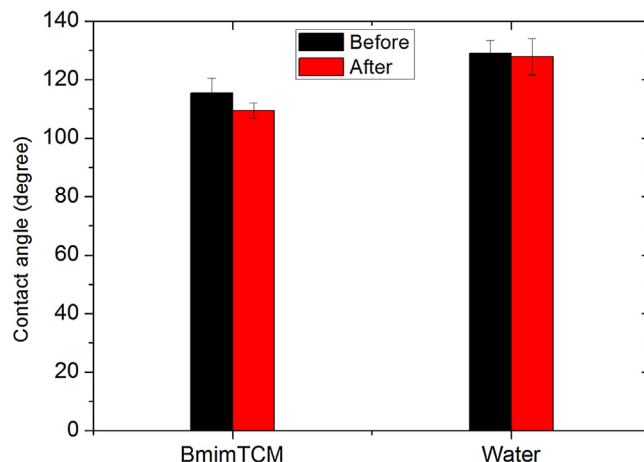


**Fig. 4.** Contact angle of [Bmim][TCM] and water on the SPG glass membrane before and after several tests.

It is commonly reported that the surface morphologies of polymeric membranes showed significant changes due to membrane wetting or degradation induced by solvents, even only after operating at room temperature and atmospheric pressure (Wang et al., 2005). In the present work, however, no evident changes could be observed after the membrane was tested at 80 °C and 20 bar [Bmim][TCM] for more than 30 h, indicating that [Bmim][TCM] has a negligible effect on the porous structure of the hydrophobic glass membrane.

Contact angle measurements were carried out to further confirm the absence of relevant pore wetting and degradation phenomena, suggested from the observation through the SEM observations. Fig. 4 shows the contact angles of the inner surface of the glass membranes using [Bmim][TCM] and water as the liquid phase before and after 10 runs of the absorption tests. There were only slight decreases in the contact angle for both [Bmim][TCM] and water before and after the tests, and the variation is within the experimental error. It is reasonable to assume that the contact angle

will not further decrease with a longer operating time, suggesting that the membrane is stable in [Bmim][TCM] for long-term testing.

Membrane wetting is one of the main challenges in a gas/liquid membrane contactor. Theoretically membrane wetting can be avoided by controlling the gas-liquid phase pressure difference within a range that can be calculated by the Young-Laplace equation. The critical entry pressure of the membrane can be calculated based on contact angle, surface tension and pore size as shown in Eq. (10) (Mosadegh-Sedghi et al., 2014):

$$\Delta P_c = -\frac{4\gamma_L \cos(\theta)}{d_p} \quad (10)$$

Where  $\Delta P_c$  represents the critical entry pressure (breakthrough pressure),  $\gamma_L$ ,  $\theta$  and  $d_p$  represent the surface tension of the liquid, the contact angle between the liquid phase and the membrane and the membrane pore diameter, respectively.

#### 4.2. Effects of operating parameters

The key operating parameters in the membrane absorption process generally include liquid and gas flow rates, operating pressure, temperature, and module geometry. In the present case, however, due to the volumetric limitation of the piston accumulator (21) used to inject the absorbent into the test rig, and the minimum time for the stabilization of the system (~30 min), the liquid flow had to be fixed as 20 ml min<sup>-1</sup>, while the gas flow rate, operating temperature, and pressure were varied to investigate their effects on the gas separation performances. The minimum testing gas flow rate is set as 50 ml min<sup>-1</sup> to obtain the real-time gas composition, as it will take more than 15 min to stabilize the gas analyzer if the gas flow rate is lower.

##### 4.2.1. Effects of operating temperature

Most of the reported membrane contactors for CO<sub>2</sub> capture operate at room temperature, as the vapor pressure of conventional solvent (e.g. MEA and water) is too high at elevated temperatures (e.g. 80 °C), and consequently the solvent loss increases significantly. However, temperature has a negligible effect on the vapor pressure of ILs in the investigated range in this study, as many ILs have their boiling points close to or even higher than their decomposition temperature (Rebelo et al., 2005). Therefore, it is possible to use ILs in a membrane contactor at elevated temperatures. In this study, the maximum testing temperature is determined to be 80 °C to ensure a sufficient absorption/desorption cyclic CO<sub>2</sub> sorption capacity (desorption at 120–140 °C). The long term stability of the sealing material (rubbery O-ring in this work) in ILs is also an important consideration.

The increase of operating temperature in IL-based absorption process has two opposite effects: on one hand, it significantly reduces the viscosity of ILs, thus promoting CO<sub>2</sub> diffusion; on the other hand, it reduces the CO<sub>2</sub> solubility in the solvent, as Henry's law constant is negatively affected by the temperature increase if no chemical reaction is involved (Lei et al., 2014; Okoturo and VanderNoot, 2004). It is of critical importance to investigate the influence of temperature on the membrane absorption process and to determine the optimal operating temperature, especially for high-temperature applications such as syngas separation in this study. As reported in (Zubeir et al., 2015), the viscosity and Henry constant of [Bmim][TCM] are both temperature dependent and follow Eqs. S(2) and S(7), respectively.

The CO<sub>2</sub> diffusivity in the liquid phase and Henry constant are calculated from the two equations, and their plots with temperature in the range of room temperature to 80 °C are shown in Fig. 6. As reported in Zubeir et al. (2015), the viscosity of [Bmim][TCM] decreases from 27.8 mPa s to 5.83 mPa s when the temperature increases from RT to 80 °C. As a consequence, the CO<sub>2</sub> diffusivity

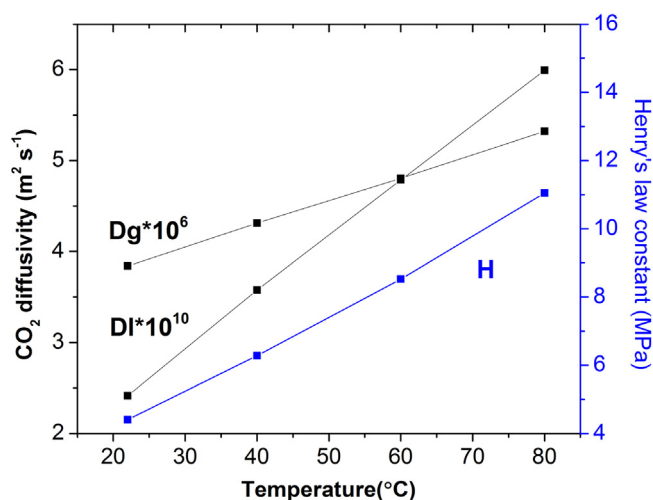


Fig. 5. Effect of temperature on CO<sub>2</sub> diffusivity and Henry's law constant. Data of viscosity and Henry's law constant was collected from ref (Zubeir et al., 2015), CO<sub>2</sub> diffusivity in the liquid side was calculated from Eq. S(6).

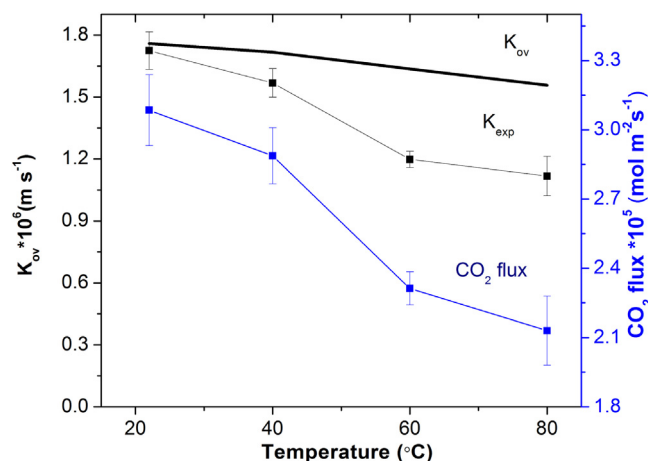


Fig. 6. Effect of temperature on  $K_{ov}$  and CO<sub>2</sub> flux. (Experimental conditions:  $Q_{gas} = 50 \text{ ml min}^{-1}$ ,  $Q_{liquid} = 20 \text{ ml min}^{-1}$ ,  $P = 1 \text{ bar}$ ).

in the liquid phase shows a two-fold increase, as can be seen in Fig. 5. The temperature increase also shows a positive effect on the gas diffusivity in the gas phase, as the  $D_g$  increases about 1.4 times. However, the Henry's law constant of [Bmim][TCM] increases from 4.84 MPa to 11.4 MPa with the temperature increasing in the investigated temperature range, indicating that temperature has a negative effect on the CO<sub>2</sub> solubility in [Bmim][TCM].

As  $K_{ov}$  is a function of  $k_l$ ,  $k_m$ , and  $k_g$ , and CO<sub>2</sub> solubility and diffusivity are the two key parameters for the three mass transfer coefficients, the effect of temperature (under atmospheric pressure) on the overall mass transfer coefficient was studied, as shown in Fig. 6. With the temperature increasing from RT to 80 °C, the overall mass transfer coefficient ( $K_{ov}$ ) estimated from the resistance in series model (shown in Equation (1)) decreases from  $1.76 \times 10^{-6} \text{ m s}^{-1}$  to  $1.56 \times 10^{-6} \text{ m s}^{-1}$ , suggesting that the CO<sub>2</sub> solubility has a larger impact on the overall mass transfer coefficient than the CO<sub>2</sub> diffusivity. A clear reduction in the  $K_{exp}$  obtained from experiment data can be also observed within the investigated temperature range. The  $K_{ov}$  fits well with the experimental data ( $K_{exp}$ ) at room temperature, but a deviation is observed for  $K_{ov}$  and  $K_{exp}$  at higher temperatures. This behavior may be attributed to the occurrence of gradual partial wetting of the membrane (penetration of the liquid into the pores of the membrane and occupying a certain

ratio of the channel), as the surface tension of the [Bmim][TCM] decreases with increasing temperature (Zubeir et al., 2015), making the penetration into the membrane pores easier. The  $K_{ov}$  from this work is about one magnitude lower than the  $K_{ov}$  obtained from aqueous amine solutions at room temperature, mainly due to two reasons; first, the absorbent in this study is a physical solvent with no chemical reaction involved (Lu et al., 2010); second, the high viscosity of the [Bmim][TCM] resulted in low gas diffusivity in the liquid phase (Dindore et al., 2004a). Nevertheless, the  $K_{ov}$  obtained from this study is comparable with the value reported in membrane contactors using other physical sorption-type ILs such as [Emim][EtSO<sub>4</sub>] (Albo et al., 2010).

Fig. 6 also shows the temperature dependence of the CO<sub>2</sub> flux in the membrane absorption process. Although CO<sub>2</sub> diffusivity increases with the increasing temperature, the CO<sub>2</sub> flux through the membrane exhibits a sharp drop at high temperatures, indicating that the CO<sub>2</sub> solubility reduction in the IL dominates the absorption process at high temperatures. The CO<sub>2</sub> flux reduces from  $3.09 \times 10^{-5} \text{ mol m}^{-2} \text{ s}^{-1}$  to  $2.13 \times 10^{-5} \text{ mol m}^{-2} \text{ s}^{-1}$  when the temperature increases from RT to 80 °C. Nevertheless, the membrane contactor shows stable separation performances even at 80 °C, while at the same temperature aqueous absorbents (e.g., amines) will suffer a high solvent loss due to the massive evaporation of the absorbents. Another common challenge in using aqueous or volatile organic solvents is the condensation of the vapors in the membrane pores and the consequent membrane wetting, which, due to ILs' intrinsic negligible vapor pressure, can be avoided when using ILs as absorbents. As the viscosity of [Bmim][TCM] is relatively low in the investigated temperature range in this study (5–30 mPa s), the viscosity has a limited influence on the diffusivity. However, if using ILs with a higher viscosity (e.g. [Bmim][PF<sub>6</sub>] and [Bmim][PF<sub>4</sub>]), the influence of viscosity in the low-temperature range should be considered.

#### 4.2.2. Effects of operating pressure

Despite a large number of publications on CO<sub>2</sub> absorption using membrane contactors, most of the reported membrane contactors operate at relatively low pressures (close to atmospheric pressure) and normally aimed at capturing CO<sub>2</sub> from flue gas. In the present study, however, the target application is syngas separation, which operates at a pressure of up to 20 bar. It is therefore important to investigate the influence of the pressure on the separation performances of the membrane contactor. When operating at elevated pressures in membrane contactors, particular attention must be paid on the control of the pressure differences between the liquid and gas phases to avoid membrane wetting. The effects of the operating pressure are studied both theoretically and through experiments. It is found to be more challenging to maintain the right pressure differences to avoid wetting at elevated pressures.

According to Eqs. S(3) and S(4), increasing operation pressure reduces the gas diffusivity in gas phase and membrane phase; a reduction of more than one magnitude was obtained for gas phase diffusivity, as shown in Fig. 7.

Nevertheless, due to the increase of driving force, a great enhancement of CO<sub>2</sub> flux with increasing pressure is observed, as shown in Fig. 8; an approximately 4–7-fold increment by increasing the operating pressure from atmospheric pressure to 20 bar was recorded at various operating temperatures (RT–80 °C).

In the low-pressure range (<10 bar) the CO<sub>2</sub> fluxes are very similar for all temperature. Little effect of temperature can be found. However, the CO<sub>2</sub> flux increases more slowly at higher temperatures (60 and 80 °C) when the pressure is above 10 bar. One reason could be the lower CO<sub>2</sub> sorption capacity at higher temperatures, and another possible explanation could be the fact that the surface tension of the ILs decreases when increasing the operating temperature, and hence the membrane wetting could be more serious

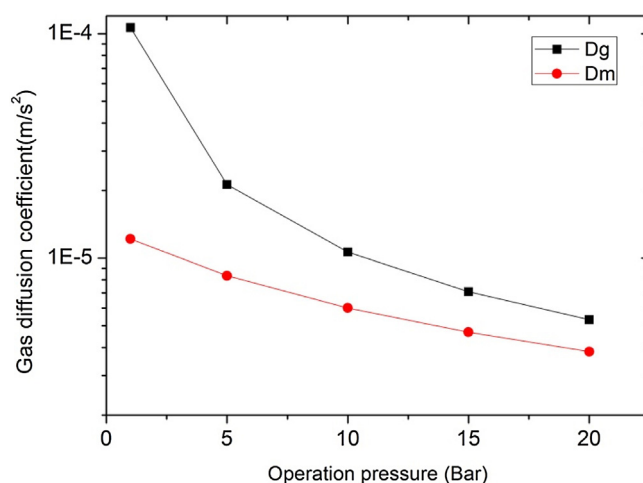


Fig. 7. Effect of operation pressure on gas and membrane phase gas diffusivity. (Experimental conditions:  $T = 80 \text{ }^\circ\text{C}$ , wetting ratio = 0,  $Q_{\text{gas}} = 50 \text{ ml min}^{-1}$ ,  $Q_{\text{liquid}} = 20 \text{ ml min}^{-1}$ ).

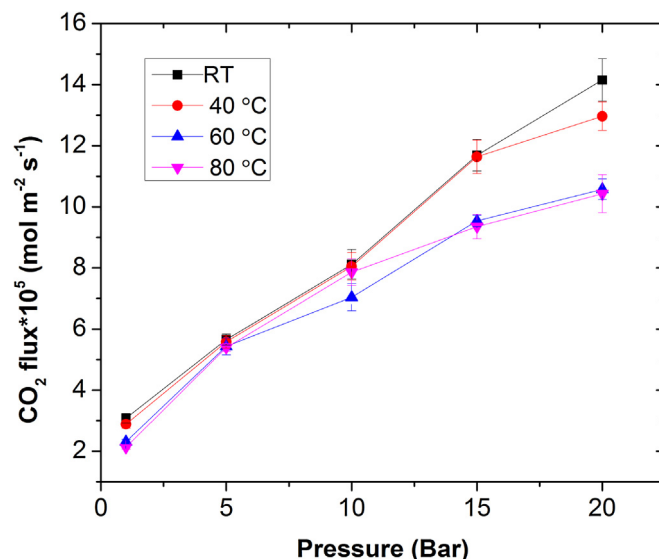
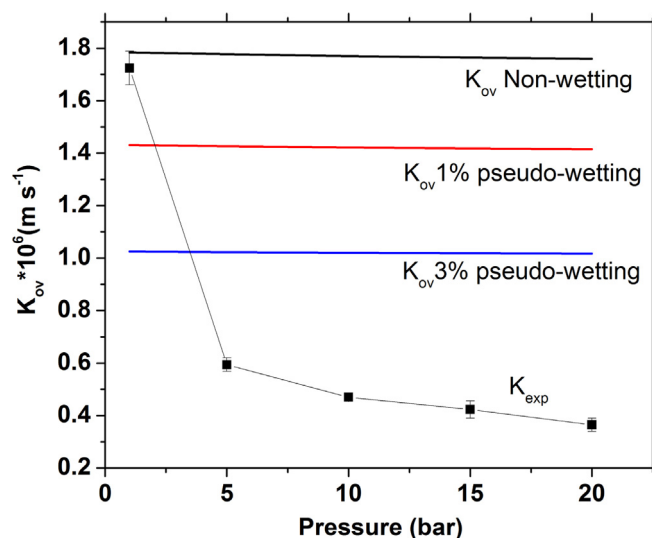


Fig. 8. Effect of operating pressure on CO<sub>2</sub> flux. (Experimental conditions:  $Q_{\text{gas}} = 50 \text{ ml min}^{-1}$ ,  $Q_{\text{liquid}} = 20 \text{ ml min}^{-1}$ ,  $T = 22 \text{ }^\circ\text{C}$ ).

at higher pressures. Nevertheless, the effects of operating pressure seem more significant than that of the temperature on the CO<sub>2</sub> flux. For example, the CO<sub>2</sub> flux decreases approx. 40% with the temperature increasing from RT to 80 °C, while at 80 °C, by increasing the operating pressure from 1 bar to 20 bar, the CO<sub>2</sub> flux increased from about  $2.12 \times 10^{-6} \text{ mol m}^{-2} \text{ s}^{-1}$  to  $10.4 \times 10^{-6} \text{ mol m}^{-2} \text{ s}^{-1}$ , corresponding to a 5-times increase.

In this study, both the CO<sub>2</sub> flux and  $K_{ov}$  are much higher compared to reported membrane contactors using other ILs (e.g., a process using [Emim][EtSO<sub>4</sub>]) (Zubeir et al., 2015). The lower viscosity of [Bmim][TCM] (27.8 mPa s at 298.2 K) (Schmidt et al., 2012) compared to [Emim][EtSO<sub>4</sub>] (97.2 mPa s at 298.2 K) may be the main contribution to this improvement (Zubeir et al., 2015). The relatively higher CO<sub>2</sub> solubility in [Bmim][TCM] Henry's law constant for [Bmim][TCM] and [Emim][EtSO<sub>4</sub>] is 5.33 MPa and 6.07 MPa at 303.2 K, respectively (Jalili et al., 2010) and (Zubeir et al., 2015) also contributes to the higher CO<sub>2</sub> fluxes.

However, the overall mass transfer coefficient retrieved by the resistance in series model ( $K_{ov}$ ) and the experimental data ( $K_{exp}$ ) does not correlate well as in the previous case at a low pressure,



**Fig. 9.** Effect of pseudo-wetting on the performance of the membrane contactor. (Experimental conditions:  $Q_{\text{gas}} = 50 \text{ ml min}^{-1}$ ,  $Q_{\text{liquid}} = 20 \text{ ml min}^{-1}$ ,  $T = 22 \text{ }^\circ\text{C}$ ).

and the theoretical flux results are always higher than the results obtained experimentally (shown in Fig. 9). Membrane wetting may start at a relatively higher pressure. To investigate the influence of pseudo-wetting at high pressures (Faiz et al., 2014),  $K_{\text{ov}}$  was also calculated by considering 1% and 3% pseudo-wetting and compared with the  $K_{\text{exp}}$ , as can be seen in Fig. 9.

As shown in Fig. 9, the 1% pseudo-wetting generates a 22% decrease in  $K_{\text{ov}}$ . When 3% pseudo-wetting conditions are considered,  $K_{\text{ov}}$  is reduced from  $1.75 \times 10^{-6} \text{ m s}^{-1}$  to  $1.02 \times 10^{-6} \text{ m s}^{-1}$ . However, this value is still much higher compared with the experimental value at 20 bar ( $0.365 \times 10^{-6} \text{ m s}^{-1}$ ). Hence, there must have been more than 3% membrane wetting in the membrane contactor at 20 bar. Extra effort must be made to prevent membrane wetting for membrane absorption at elevated pressures. It is important to control the pressure difference through the porous membrane to be lower than the membrane wetting pressures. By using the contact angle (over  $105^\circ$  at RT), membrane pore size (100 nm) and [Bmim][TCM] surface tension ( $\sim 47 \text{ mN m}^{-1}$  at RT (Zubeir et al., 2015)), the critical entry pressure can be calculated from Eq. (10) (Mosadegh-Sedghi et al., 2014). For the glass membrane used in this study, the penetration pressure is over 5 bar by calculation. In addition, the liquid phase pressure drop (lower than 0.3 bar) and gas phase pressure drop (lower than 0.2 bar) along the membrane module were obtained in the experimental system. However, even though the gas and liquid stream outlet pressures of the membrane module were carefully controlled to be the same (the maximum pressure difference between gas and liquid phase is lower than 0.5 bar), membrane wetting was still observed. One possible reason is the existing of the membrane defects. The leaked ILs into the gas phase through the defects may block some pores from the gas side of the membrane and causing partial wetting. One option to reduce/avoid membrane wetting is to use thin film composite membrane with a dense top layer (Scholes et al., 2015); it is studied in another project and a comparison of the two processes was reported elsewhere (Dai et al., 2016b).

Theoretically the increase in operating pressures can reduce the overall mass transfer resistance, as the gas diffusivities in both gas and membrane phase decrease with the increase of pressure, and consequently the  $k_g$  and  $k_m$  are both reduced at a higher pressure. The effect of operation pressure on the mass transfer coefficients can be seen in Fig. 10(A).

The estimated percentage mass transfer resistances are given in Fig. 10(B). The impact of operating pressure on the overall mass

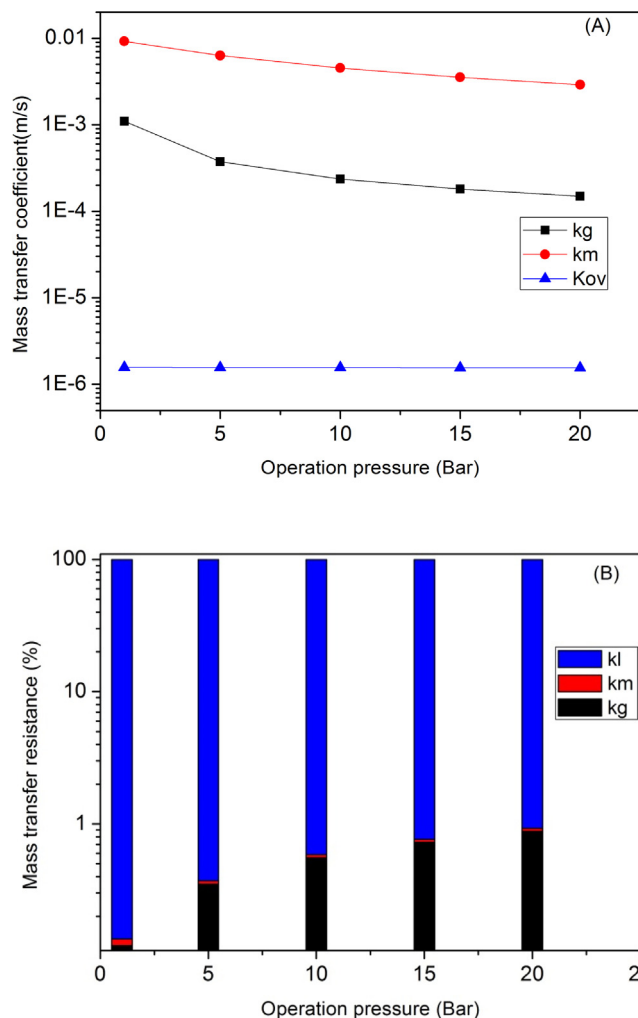


**Fig. 10.** Effect of operation pressure on mass transfer coefficient (A) and percentage mass transfer resistance (B) in gas and membrane phase. (Experimental conditions:  $T = 80 \text{ }^\circ\text{C}$ , wetting ratio = 0,  $Q_{\text{gas}} = 50 \text{ ml min}^{-1}$ ,  $Q_{\text{liquid}} = 20 \text{ ml min}^{-1}$ ).

transfer coefficient seems not significant based on the calculation;  $K_{\text{ov}}$  remains nearly constant along the investigated pressure range as the overall mass transfer resistance is mainly contributed by the liquid phase. Conversely,  $K_{\text{exp}}$  from the experiment (presented in Fig. 9) decreases dramatically as the operating pressure increases, suggesting that wetting probably have taken place under higher pressures. Membrane wetting can largely reduce the mass transfer coefficient in membrane phase and the overall mass transfer coefficient (Fig. 11(A)). Within only 1% and 3% pseudo-wetting, the contribution of membrane phase in the overall mass transfer resistance significantly increases, as shown in Fig. 11(B).

#### 4.2.3. Effects of the gas flow rate

Another key parameter in membrane absorption processes is the gas flow rate inside the membrane module. Fig. 12 shows the  $\text{CO}_2$  fluxes and overall mass transfer coefficients as a function of gas flow rate at 20 bar and  $80 \text{ }^\circ\text{C}$ .

As expected, the  $\text{CO}_2$  flux increases significantly as the gas flow rate increases from  $50 \text{ ml min}^{-1}$  to  $200 \text{ ml min}^{-1}$ , as can be seen from Fig. 13.  $K_{\text{exp}}$  also significantly increases with the increasing gas flow rate. This suggests that a relatively high gas flow may effectively enhance mass transfer. However, in practice the gas flow rate needs to be optimized to maintain a high  $\text{CO}_2$  removal efficiency and meet the outlet gas specification. It is worth mentioning that even with a gas flow rate at  $200 \text{ ml min}^{-1}$ ,  $K_{\text{exp}}$  is still lower than

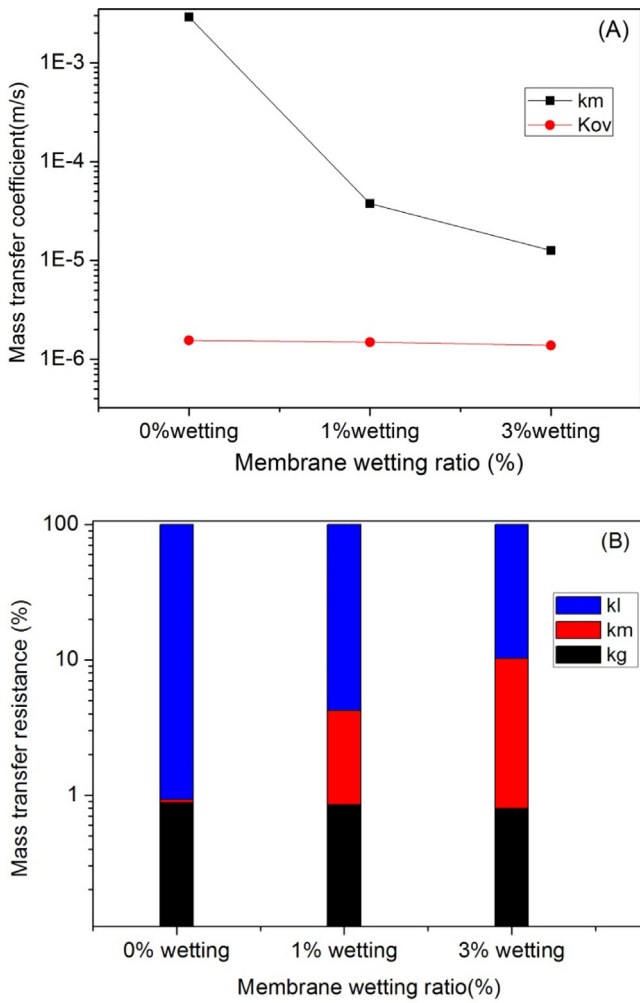


**Fig. 11.** Effect of wetting ratio on mass transfer resistance in gas and membrane phase (A) and percentage mass transfer resistance (B). (Experimental conditions:  $T = 80^\circ\text{C}$ ,  $P = 20\text{ bar}$ ,  $Q_{\text{gas}} = 50\text{ ml min}^{-1}$ ,  $Q_{\text{liquid}} = 20\text{ ml min}^{-1}$ ).

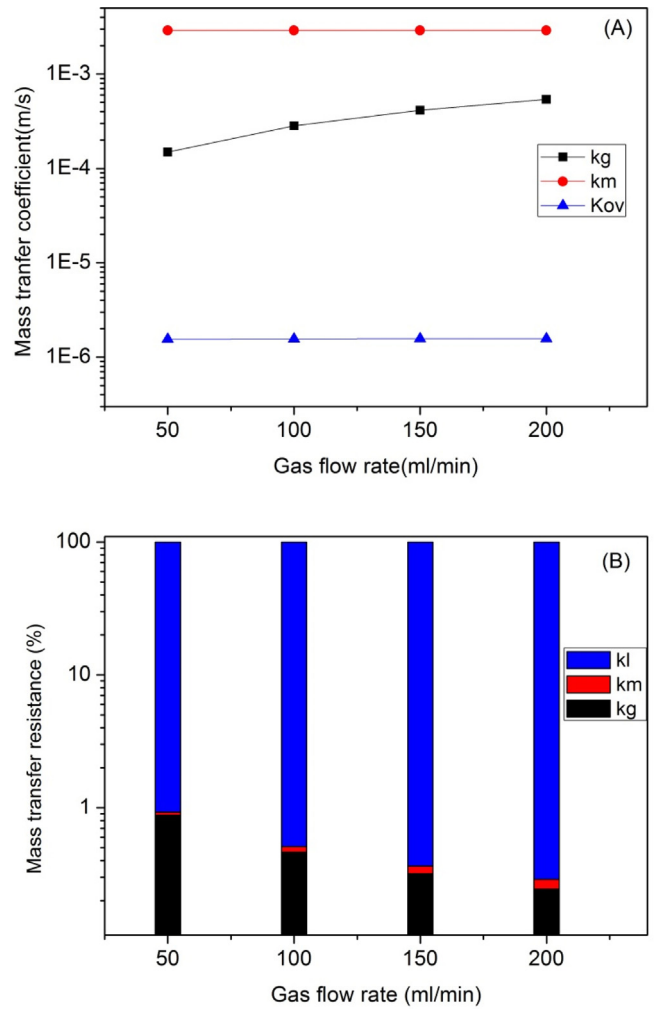


**Fig. 13.** Effect of gas flow rate on mass transfer coefficient in gas and membrane phase (a) and percentage mass transfer resistance (b). Operation conditions:  $T = 80^\circ\text{C}$ , wetting ratio = 0,  $P = 20\text{ bar}$ ,  $Q_{\text{liquid}} = 20\text{ ml min}^{-1}$ .

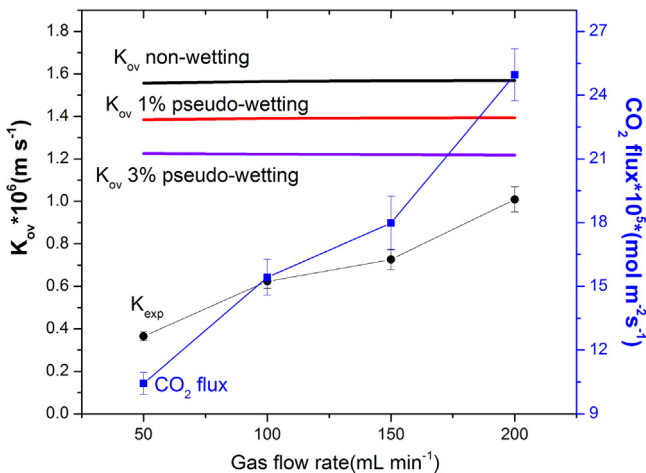


**Fig. 12.** Effect of gas flow rate on  $\text{CO}_2$  flux and overall mass transfer coefficient. (Experimental conditions:  $P = 20\text{ bar}$ ,  $T = 80^\circ\text{C}$ ,  $Q_{\text{liquid}} = 20\text{ ml min}^{-1}$ ).

$K_{\text{ov}}$  estimated from resistance in series model when considering the pseudo-wetting, indicating the occurrence of partial membrane wetting.

Generally, a higher gas flow rate leads to higher  $\text{CO}_2$  flux as it offers a higher overall mass transfer coefficient on the gas phase,

as shown in Fig. 13(A). However, the contribution of the gas phase mass transfer resistance is not significant to the overall mass transfer resistance (see Fig. 13(B)), which explains that increasing gas flow rate has limited enhancement effect on the overall mass transfer coefficient ( $K_{\text{ov}}$ ).

Generally speaking, the liquid side mass flow rate should give more significant influence on the overall mass transfer than the gas flow rate. However, due to the limitation of the piston accumulator and the time need to stabilize the system and ensure the steady state, in this study the liquid flow rate had to be fixed at  $20\text{ ml min}^{-1}$ . Nevertheless, attempts have been made to put a cylindrical spacer into the center of the glass membrane in order to increase the liquid flow rate and promote the liquid side turbulence. Indeed, the liquid phase mass transfer was enhanced remarkably; the  $\text{CO}_2$  flux is around 1.3–1.5 times higher than membrane contactor without spacer at the same operation conditions. However, the liquid phase pressure drop along the membrane module increases significantly as well, which makes it extremely difficult to control the pressure balance and avoid membrane wetting. The optimization of the membrane module configuration will be studied in the future work.

## 5. Conclusion

This work investigated the separation performances of an ionic liquid based membrane contactor for pre-combustion CO<sub>2</sub> capture at elevated temperatures and pressures. [Bmim][TCM] was selected as the effective absorbent in the process. Experimental overall mass transfer coefficients ( $K_{exp}$ ) of  $0.365\text{--}1.01 \times 10^{-6} \text{ m s}^{-1}$  were obtained at elevated pressure (20 bar) and temperature (80 °C), while due to the big driving force offered by the relatively high operating pressure, a CO<sub>2</sub> flux of  $10.4\text{--}24.9 \times 10^{-6} \text{ mol m}^{-2} \text{ s}^{-1}$  were obtained. Experimental overall mass transfer coefficients ( $K_{exp}$ ) and model predictions ( $K_{ov}$ ) show good agreement at low pressures. However, deviations were observed at higher operating pressures, indicating the occurrence of membrane wetting in the membrane contactor. It is found that operating pressure plays the key role while temperature has a much less significant effect on the membrane contactor separation performance.

However, experimental results show that the membrane contactor has undergone wetting problems at high pressures in this work, which makes the process less efficient. It is therefore of great importance to prevent membrane wetting to ensure high separation efficiency. The use of membranes with a highly CO<sub>2</sub> permeable thin non-porous top layer may eliminate membrane wetting while keeping a low mass transfer resistance: this study is still on-going.

## Acknowledgements

This work is supported by the Research Council of Norway through the CLIMIT program (No. 215732). The authors also want to acknowledge Prof. Hallvard Svendsen and Dr. Arne Lindbråthen for the inspiring discussions.

## Appendix A. Supplementary data

Supplementary data associated with this article can be found, in the online version, at <http://dx.doi.org/10.1016/j.ijggc.2016.09.001>.

## References

- Abanades, J.C., Arias, B., Lyngfelt, A., Mattisson, T., Wiley, D.E., Li, H., Ho, M.T., Mangano, E., Brandani, S., 2015. Emerging CO<sub>2</sub> capture systems. *Int. J. Greenh. Gas Control* 40, 126–166.
- Ahmad, A.L., Sunarti, A.R., Lee, K.T., Fernando, W.J.N., 2010. CO<sub>2</sub> removal using membrane gas absorption. *Int. J. Greenh. Gas Control* 4, 495–498.
- Albo, J., Irabien, A., 2012. Non-dispersive absorption of CO<sub>2</sub> in parallel and cross-flow membrane modules using EMISE. *J. Chem. Technol. Biot.* 87, 1502–1507.
- Albo, J., Luis, P., Irabien, A., 2010. Carbon dioxide capture from flue gases using a cross-flow membrane contactor and the ionic liquid 1-ethyl-3-methylimidazolium ethylsulfate. *Ind. Eng. Chem. Res.* 49, 11045–11051.
- Albo, J., Luis, P., Irabien, A., 2011. Absorption of coal combustion flue gases in ionic liquids using different membrane contactors. *Desalin. Water Treat.* 27, 54–59.
- Anderson, J.L., Dixon, J.K., Brennecke, J.F., 2007. Solubility of CO<sub>2</sub>, CH<sub>4</sub>, C<sub>2</sub>H<sub>6</sub>, C<sub>2</sub>H<sub>4</sub>, O<sub>2</sub>, and N<sub>2</sub> in 1-hexyl-3-methylpyridinium bis(trifluoromethylsulfonyl)imide: comparison to other ionic liquids. *Acc. Chem. Res.* 40, 1208–1216.
- Anthony, J.L., Maginn, E.J., Brennecke, J.F., 2002a. Solubilities and thermodynamic properties of gases in the ionic liquid 1-n-butyl-3-methylimidazolium hexafluorophosphate. *J. Phys. Chem. B* 106, 7315–7320.
- Anthony, J.L., Maginn, E.J., Brennecke, J.F., 2002b. Solubilities and thermodynamic properties of gases in the ionic liquid 1-n-butyl-3-methylimidazolium hexafluorophosphate. *J. Phys. Chem. B* 106, 7315–7320.
- Anthony, J.L., Anderson, J.L., Maginn, E.J., Brennecke, J.F., 2005. Anion effects on gas solubility in ionic liquids. *J. Phys. Chem. B* 109, 6366–6374.
- Ayala, A.E., Simoni, L.D., Lin, Y.D., Brennecke, J.F., Stadtherr, M.A., 2006. Process design using ionic liquids: physical property modeling. *Comput. Aided Chem. Eng.* 21, 463–468.
- Bara, J.E., Gabriel, C.J., Hatakeyama, E.S., Carlisle, T.K., Lessmann, S., Noble, R.D., Gin, D.L., 2008. Improving CO<sub>2</sub> selectivity in polymerized room-temperature ionic liquid gas separation membranes through incorporation of polar substituents. *J. Membrane Sci.* 321, 3–7.
- Bara, J.E., Carlisle, T.K., Gabriel, C.J., Camper, D., Finotello, A., Gin, D.L., Noble, R.D., 2009. Guide to CO<sub>2</sub> separations in imidazolium-based room-temperature ionic liquids. *Ind. Eng. Chem. Res.* 48, 2739–2751.
- Boributh, S., Assabumrungrat, S., Laosiripojana, N., Jiratananon, R., 2011. A modeling study on the effects of membrane characteristics and operating parameters on physical absorption of CO<sub>2</sub> by hollow fiber membrane contactor. *J. Membrane Sci.* 380, 21–33.
- Cadogan, S.P., Maitland, G.C., Trusler, J.P.M., 2014. Diffusion coefficients of CO<sub>2</sub> and N<sub>2</sub> in water at temperatures between 298.15 K and 423.15 K at pressures up to 45 MPa. *J. Chem. Eng. Data* 59, 519–525.
- Camper, D., Bara, J., Koval, C., Noble, R., 2006. Bulk-fluid solubility and membrane feasibility of Rmim-based room-temperature ionic liquids. *Ind. Eng. Chem. Res.* 45, 6279–6283.
- Carvalho, P.J., Alvarez, V.H., Marrucho, I.M., Aznar, M., Coutinho, J.A.P., 2009. High pressure phase behavior of carbon dioxide in 1-butyl-3-methylimidazolium bis(trifluoromethylsulfonyl)imide and 1-butyl-3-methylimidazolium dicyanamide ionic liquids. *J. Supercrit. Fluid* 50, 105–111.
- Chau, J., Jie, X., Sirkar, K.K., 2015. Polyamidoamine-facilitated poly(ethylene glycol)/ionic liquid based pressure swing membrane absorption process for CO<sub>2</sub> removal from shifted syngas. *Chem. Eng. J.*
- Dai, Z., Ansaloni, L., Deng, L., 2016a. Recent advances in multi-layer composite polymeric membranes for CO<sub>2</sub> separation: a review. *Green Energy Environ.*
- Dai, Z., Noble, R.D., Gin, D.L., Zhang, X., Deng, L., 2016b. Combination of ionic liquids with membrane technology: a new approach for CO<sub>2</sub> separation. *J. Membrane Sci.* 497, 1–20.
- Dai, Z.D., Ansaloni, L., Deng, L.Y., 2016c. Precombustion CO<sub>2</sub> capture in polymeric hollow fiber membrane contactors using ionic liquids: porous membrane versus nonporous composite membrane. *Ind. Eng. Chem. Res.* 55, 5983–5992.
- Dindore, V.Y., Brilman, D.W.F., Feron, P.H.M., Versteeg, G.F., 2004a. CO<sub>2</sub> absorption at elevated pressures using a hollow fiber membrane contactor. *J. Membrane Sci.* 235, 99–109.
- Dindore, V.Y., Brilman, D.W.F., Geuzebroek, F.H., Versteeg, G.F., 2004b. Membrane-solvent selection for CO<sub>2</sub> removal using membrane gas-liquid contactors. *Sep. Purif. Technol.* 40, 133–145.
- Erdmenger, T., Vitz, J., Wiesbrock, F., Schubert, U.S., 2008. Influence of different branched alkyl side chains on the properties of imidazolium-based ionic liquids. *J. Mater. Chem.* 18, 5267–5273.
- Faiz, R., Li, K., Al-Marzouqi, M., 2014. H<sub>2</sub>S absorption at high pressure using hollow fibre membrane contactors. *Chem. Eng. Process.* 83, 33–42.
- Fredlake, C.P., Crosthwaite, J.M., Hert, D.G., Aki, S.N.V.K., Brennecke, J.F., 2004. Thermophysical properties of imidazolium-based ionic liquids. *J. Chem. Eng. Data* 49, 954–964.
- Gomez-Coma, L., Garea, A., Irabien, A., 2014. Non-dispersive absorption of CO<sub>2</sub> in [emim][EtSO<sub>4</sub>] and [emim][Ac]: temperature influence. *Sep. Purif. Technol.* 132, 120–125.
- Hasib-ur-Rahman, M., Bouteldja, H., Fongarland, P., Siaj, M., Larachi, F., 2012. Corrosion behavior of carbon steel in alkanolamine/room-temperature ionic liquid based CO<sub>2</sub> capture systems. *Ind. Eng. Chem. Res.* 51, 8711–8718.
- Huddleston, J.G., Visser, A.E., Reichert, W.M., Willauer, H.D., Broker, G.A., Rogers, R.D., 2001. Characterization and comparison of hydrophilic and hydrophobic room temperature ionic liquids incorporating the imidazolium cation. *Green Chem.* 3, 156–164.
- Iliuta, I., Bougie, F., Iliuta, M.C., 2015. CO<sub>2</sub> removal by single and mixed amines in a hollow-fiber membrane module-investigation of contactor performance. *AIChE J.* 61, 955–971.
- Jacquemin, J., Gomes, M.F.C., Husson, P., Majer, V., 2006. Solubility of carbon dioxide, ethane, methane, oxygen, nitrogen, hydrogen, argon, and carbon monoxide in 1-butyl-3-methylimidazolium tetrafluoroborate between temperatures 283 K and 343 K and at pressures close to atmospheric. *J. Chem. Thermodyn.* 38, 490–502.
- Jacquemin, J., Husson, P., Majer, V., Gomes, M.F.C., 2007. Influence of the cation on the solubility of CO<sub>2</sub> and H<sub>2</sub> in ionic liquids based on the bis(trifluoromethylsulfonyl)imide anion. *J. Solution Chem.* 36, 967–979.
- Jalili, A.H., Mehdizadeh, A., Shokouhi, M., Ahmadi, A.N., Hosseini-Jenab, M., Fateminassab, F., 2010. Solubility and diffusion of CO<sub>2</sub> and H<sub>2</sub>S in the ionic liquid 1-ethyl-3-methylimidazolium ethylsulfate. *J. Chem. Thermodyn.* 42, 1298–1303.
- Jie, X., Chau, J., Obuskovic, G., Sirkar, K.K., 2013. Preliminary studies of CO<sub>2</sub> removal from precombustion syngas through pressure swing membrane absorption process with ionic liquid as absorbent. *Ind. Eng. Chem. Res.* 52, 8783–8799.
- Jie, X.M., Chau, J., Obuskovic, G., Sirkar, K.K., 2014. Enhanced pressure swing membrane absorption process for CO<sub>2</sub> removal from shifted syngas with dendrimer-ionic liquid mixtures as absorbent. *Ind. Eng. Chem. Res.* 53, 3305–3320.
- Khaisri, S., Demontigny, D., Tontiwachwuthikul, P., Jiratananon, R., 2009. Comparing membrane resistance and absorption performance of three different membranes in a gas absorption membrane contactor. *Sep. Purif. Technol.* 65, 290–297.
- Kim, S.T., Kang, J.W., Lee, J.S., Min, B.M., 2011. Analysis of the heat of reaction and regeneration in alkanolamine-CO(2) system. *Korean J. Chem. Eng.* 28, 2275–2281.
- Koonaphtleert, S., Li, K., 2007. Preparation and characterization of hydrophobic ceramic hollow fibre membrane. *J. Membrane Sci.* 291, 70–76.
- Kreulen, H., Smolders, C.A., Versteeg, G.F., Vanswaaij, W.P.M., 1993. Determination of mass-transfer rates in wetted and non-wetted microporous membranes. *Chem. Eng. Sci.* 48, 2093–2102.

- Kurnia, K.A., Harris, F., Wilfred, C.D., Mutalib, M.I.A., Murugesan, T., 2009. Thermodynamic properties of CO<sub>2</sub> absorption in hydroxyl ammonium ionic liquids at pressures of (100–1600) kPa. *J. Chem. Thermodyn.* 41, 1069–1073.
- Lei, Z., Dai, C., Chen, B., 2014. Gas solubility in ionic liquids. *Chem. Rev.* 114, 1289–1326.
- Li, J.L., Chen, B.H., 2005. Review Of CO<sub>2</sub> absorption using chemical solvents in hollow fiber membrane contactors. *Sep. Purif. Technol.* 41, 109–122.
- Li, J., Dai, Z.D., Usman, M., Qi, Z.W., Deng, L.Y., 2016. CO<sub>2</sub>/H<sub>2</sub> separation by amino-acid ionic liquids with polyethylene glycol as co-solvent. *Int. J. Greenh. Gas Control* 45, 207–215.
- Lu, J.G., Ji, Y., Zhang, H., Chen, M.D., 2010. CO<sub>2</sub> capture using activated amino acid salt solutions in a membrane contactor. *Sep. Sci. Technol.* 45, 1240–1251.
- Lu, J.G., Lu, C.T., Chen, Y., Gao, L., Zhao, X., Zhang, H., Xu, Z.W., 2014. CO<sub>2</sub> capture by membrane absorption coupling process: application of ionic liquids. *Appl. Energy* 115, 573–581.
- Luis, P., Garea, A., Irabien, A., 2009. Zero solvent emission process for sulfur dioxide recovery using a membrane contactor and ionic liquids. *J. Membrane Sci.* 330, 80–89.
- Makhloufi, C., Lasseguette, E., Remigy, J.C., Belaisaoui, B., Roizard, D., Favre, E., 2014. Ammonia based CO<sub>2</sub> capture process using hollow fiber membrane contactors. *J. Membrane Sci.* 455, 236–246.
- McHale, G., Hardacre, C., Ge, R., Doy, N., Allen, R.W.K., MacInnes, J.M., Bown, M.R., Newton, M.I., 2008. Density-viscosity product of small-volume ionic liquid samples using quartz crystal impedance analysis. *Anal. Chem.* 80, 5806–5811.
- Mosadegh-Sedghi, S., Rodrigue, D., Brisson, J., Iliuta, M.C., 2014. Wetting phenomenon in membrane contactors – causes and prevention. *J. Membrane Sci.* 452, 332–353.
- Ohno, H., Yoshizawa, M., 2002. Ion conductive characteristics of ionic liquids prepared by neutralization of alkylimidazoles. *Solid State Ionics* 154, 303–309.
- Okoturo, O.O., VanderNoot, T.J., 2004. Temperature dependence of viscosity for room temperature ionic liquids. *J. Electroanal. Chem.* 568, 167–181.
- Ortiz, A., Gorri, D., Irabien, A., Ortiz, I., 2010. Separation of propylene/propane mixtures using Ag<sup>+</sup>-RTIL solutions. Evaluation and comparison of the performance of gas-liquid contactors. *J. Membrane Sci.* 360, 130–141.
- Papatryfon, X.L., Heliopoulos, N.S., Molchan, I.S., Zubeir, L.F., Bezemer, N.D., Arfanis, M.K., Kontos, A.G., Likodimos, V., Iliev, B., Romanos, G.E., Falaras, P., Stamatakis, K., Beltsios, K.G., Kroon, M.C., Thompson, G.E., Klockner, J., Schubert, T.J.S., 2014. CO<sub>2</sub> capture efficiency, corrosion properties, and ecotoxicity evaluation of amine solutions involving newly synthesized ionic liquids. *Ind. Eng. Chem. Res.* 53, 12083–12102.
- Ramdin, M., de Loos, T.W., Vlucht, T.J.H., 2012. State-of-the-art of CO<sub>2</sub> capture with ionic liquids. *Ind. Eng. Chem. Res.* 51, 8149–8177.
- Rebello, L.P.N., Lopes, J.N.C., Esperanca, J.M.S.S., Filipe, E., 2005. On the critical temperature, normal boiling point, and vapor pressure of ionic liquids. *J. Phys. Chem. B* 109, 6040–6043.
- Saeed, M., Deng, L.Y., 2016. Post-combustion CO<sub>2</sub> membrane absorption promoted by mimic enzyme. *J. Membrane Sci.* 499, 36–46.
- Schmidt, H., Stephan, M., Safarov, J., Kul, I., Nocke, J., Abdulagatov, I.M., Hassel, E., 2012. Experimental study of the density and viscosity of 1-ethyl-3-methylimidazolium ethyl sulfate. *J. Chem. Thermodyn.* 47, 68–75.
- Scholes, C.A., Smith, K.H., Kentish, S.E., Stevens, G.W., 2010. CO<sub>2</sub> capture from pre-combustion processes-strategies for membrane gas separation. *Int. J. Greenh. Gas Control* 4, 739–755.
- Scholes, C.A., Kentish, S.E., Stevens, G.W., deMontigny, D., 2015. Comparison of thin film composite and microporous membrane contactors for CO<sub>2</sub> absorption into monoethanolamine. *Int. J. Greenh. Gas Control* 42, 66–74.
- Sharma, A., Julcour, C., Kelkar, A.A., Deshpande, R.M., Delmas, H., 2009. Mass transfer and solubility of CO and H<sub>2</sub> in ionic liquid: case of [Bmim][PF<sub>6</sub>] with gas-Inducing stirrer reactor. *Ind. Eng. Chem. Res.* 48, 4075–4082.
- Tokuda, H., Hayamizu, K., Ishii, K., Susan, M.A.B.H., Watanabe, M., 2005. Physicochemical properties and structures of room temperature ionic liquids. 2. Variation of alkyl chain length in imidazolium cation. *J. Phys. Chem. B* 109, 6103–6110.
- Tomida, D., Kumagai, A., Qiao, K., Yokoyama, C., 2006. Viscosity of [bmim][PF<sub>6</sub>] and [bmim][BF<sub>4</sub>] at high pressure. *Int. J. Thermophys.* 27, 39–47.
- Vladislavjevic, G.T., Shimizu, M., Nakashima, T., 2005. Permeability of hydrophilic and hydrophobic Shirasu-porous-glass (SPG) membranes to pure liquids and its microstructure. *J. Membrane Sci.* 250, 69–77.
- Wang, R., Li, D.F., Liang, D.T., 2004. Modeling of CO<sub>2</sub> capture by three typical amine solutions in hollow fiber membrane contactors. *Chem. Eng. Process.* 43, 849–856.
- Wang, R., Zhang, H.Y., Feron, P.H.M., Liang, D.T., 2005. Influence of membrane wetting on CO<sub>2</sub> capture in microporous hollow fiber membrane contactors. *Sep. Purif. Technol.* 46, 33–40.
- Wang, Z., Fang, M.X., Ma, Q.H., Yu, H., Wei, C.C., Luo, Z.Y., 2014. Investigation of membrane wetting in different absorbents at elevated temperature for carbon dioxide capture. *J. Membrane Sci.* 455, 219–228.
- Wang, J., Luo, J., Feng, S., Li, H., Wan, Y., Zhang, X., 2016. Recent development of ionic liquid membranes. *Green Energy Environ.*
- Wappel, D., Gronald, G., Kalb, R., Draxler, J., 2010. Ionic liquids for post-combustion CO<sub>2</sub> absorption. *Int. J. Greenh. Gas Control* 4, 486–494.
- Xu, G.S., Yao, J.F., Wang, K., He, L., Webley, P.A., Chen, C.S., Wang, H.T., 2011. Preparation of ZIF-8 membranes supported on ceramic hollow fibers from a concentrated synthesis gel. *J. Membrane Sci.* 385, 187–193.
- Yang, M.C., Cussler, E.L., 1986. Designing hollow-fiber contactors. *AIChE J.* 32, 1910–1916.
- Yang, H.Q., Xu, Z.H., Fan, M.H., Gupta, R., Slimane, R.B., Bland, A.E., Wright, I., 2008. Progress in carbon dioxide separation and capture: a review. *J. Environ. Sci. China* 20, 14–27.
- Yokozeki, A., Shiflett, M.B., 2007. Hydrogen purification using room-temperature ionic liquids. *Appl. Energy* 84, 351–361.
- Yokozeki, A., Shiflett, M.B., Junk, C.P., Grieco, L.M., Foo, T., 2008. Physical and chemical absorptions of carbon dioxide in room-temperature ionic liquids. *J. Phys. Chem. B* 112, 16654–16663.
- Yong, J.K.J., Stevens, G.W., Caruso, F., Kentish, S.E., 2015. The use of carbonic anhydrase to accelerate carbon dioxide capture processes. *J. Chem. Technol. Biot.* 90, 3–10.
- Zhang, X.P., Zhang, X.C., Dong, H.F., Zhao, Z.J., Zhang, S.J., Huang, Y., 2012. Carbon capture with ionic liquids: overview and progress. *Energy Environ. Sci.* 5, 6668–6681.
- Zhang, Y., Sunarso, J., Liu, S.M., Wang, R., 2013. Current status and development of membranes for CO<sub>2</sub>/CH<sub>4</sub> separation: a review. *Int. J. Greenh. Gas Control* 12, 84–107.
- Zubeir, L.F., Romanos, G.E., Weggemans, W.M.A., Iliev, B., Schubert, T.J.S., Kroon, M.C., 2015. Solubility and diffusivity of CO<sub>2</sub> in the ionic liquid 1-butyl-3-methylimidazolium tricyanomethanide within a large pressure range (0.01 MPa–10 MPa). *J. Chem. Eng. Data* 60, 1544–1562.